Supplemental Information

# Investigation of Interaction between MXene Nanosheets and Human Plasma and Protein Corona Composition

Xuri Wu, Feng Tan*, Shizhu Cheng, Yangyang Chang, Xiaochun Wang, Lingxin Chen*

X. R. Wu, F. Tan, S. Z. Cheng, Y. Y. Chang

Key Laboratory of Industrial Ecology and Environmental Engineering (MOE)

School of Environmental Science and Technology

Dalian University of Technology

Dalian 116024, P. R. China

E-mail: tanf@dlut.edu.cn

X. C. Wang

Shandong Provincial Key Laboratory of Biochemical Engineering

College of Marine Science and Biological Engineering

Qingdao University of Science and Technology

Qingdao 266042, P. R. China

L. X. Chen

CAS Key Laboratory of Coastal Environmental Processes and Ecological Remediation

Yantai Institute of Coastal Zone Research

Chinese Academy of Sciences

Yantai 264003, P. R. China

E-mail: lxchen@yic.ac.cn
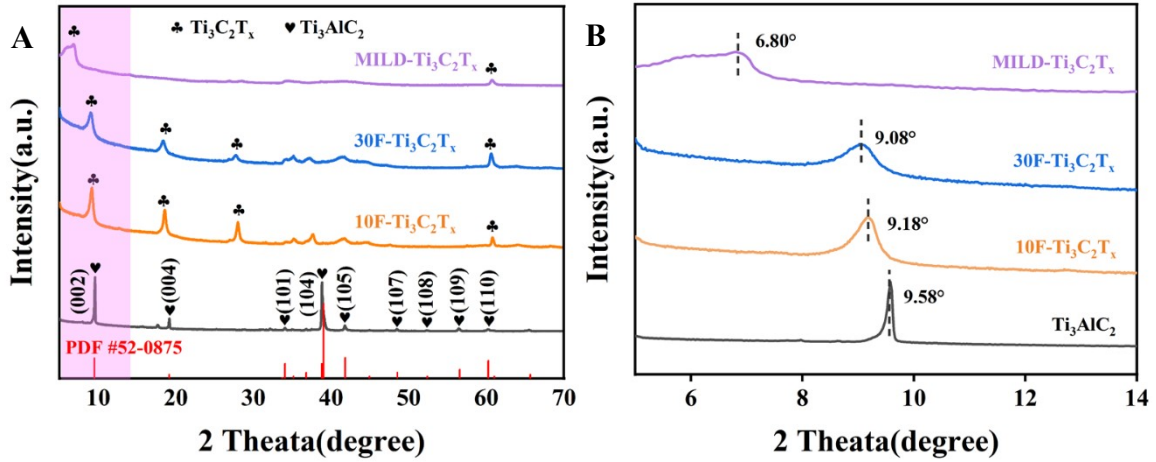
Supplemental Figure 1. XRD patterns of Ti_3AlC_2 and etched productions (A) treated in 10 wt% ($10F-Ti_3C_2T_x$), 30 wt% ($30F-Ti_3C_2T_x$) concentrated HF solution, and LiF/HCl mixed solution ($MILD-Ti_3C_2T_x$); (B) magnification of (0 0 2) peak in (A).
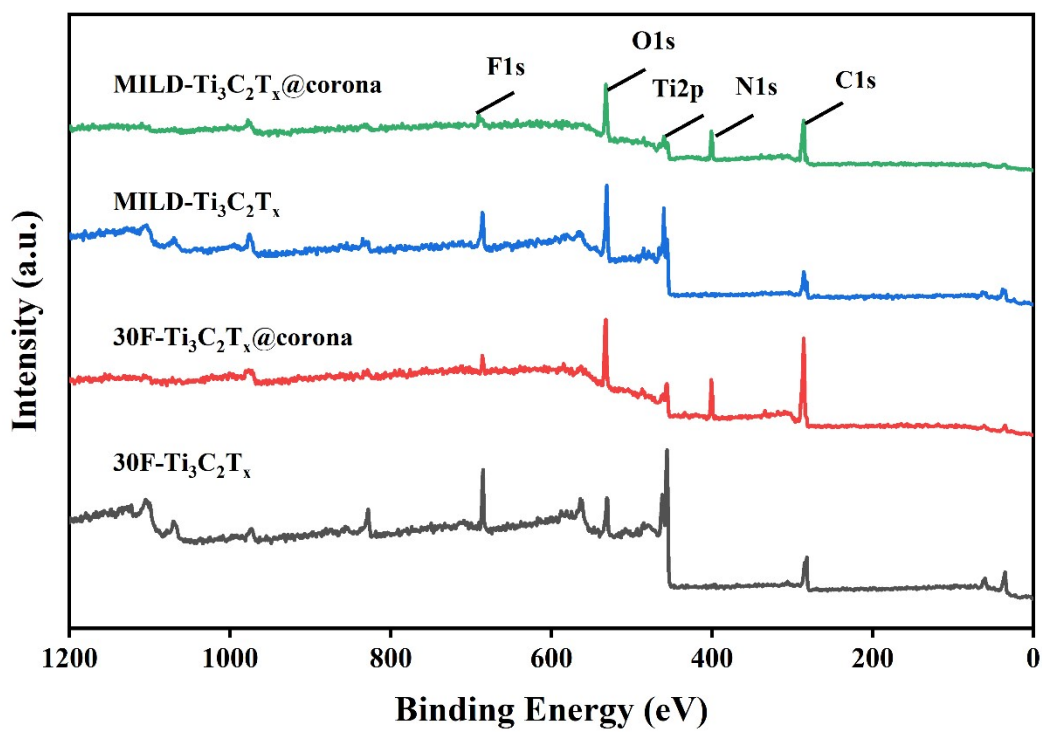
Supplemental Figure 2. XPS survey spectra of all samples including 30F-$Ti_3C_2T_x$ and 30F-$Ti_3C_2T_x$@corona, MILD-$Ti_3C_2T_x$, and MILD-$Ti_3C_2T_x$@corona.
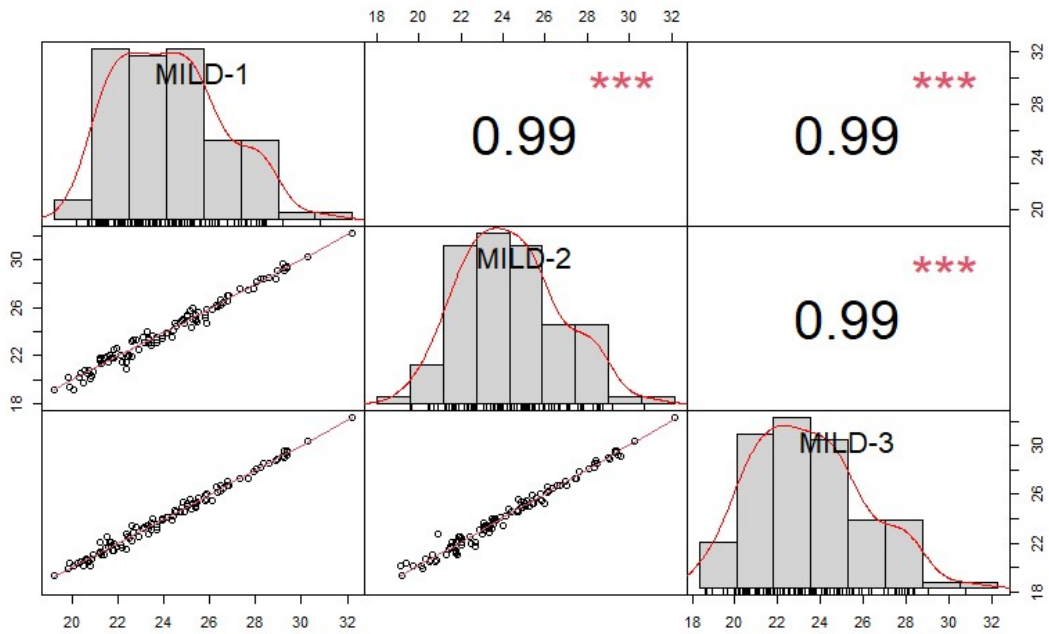
Supplemental Figure 3. Correlation matrix diagram in three repetitions of sample loading. Excellent correlations were shown, indicating the excellent performance and reproducibility of the mass spectrum.
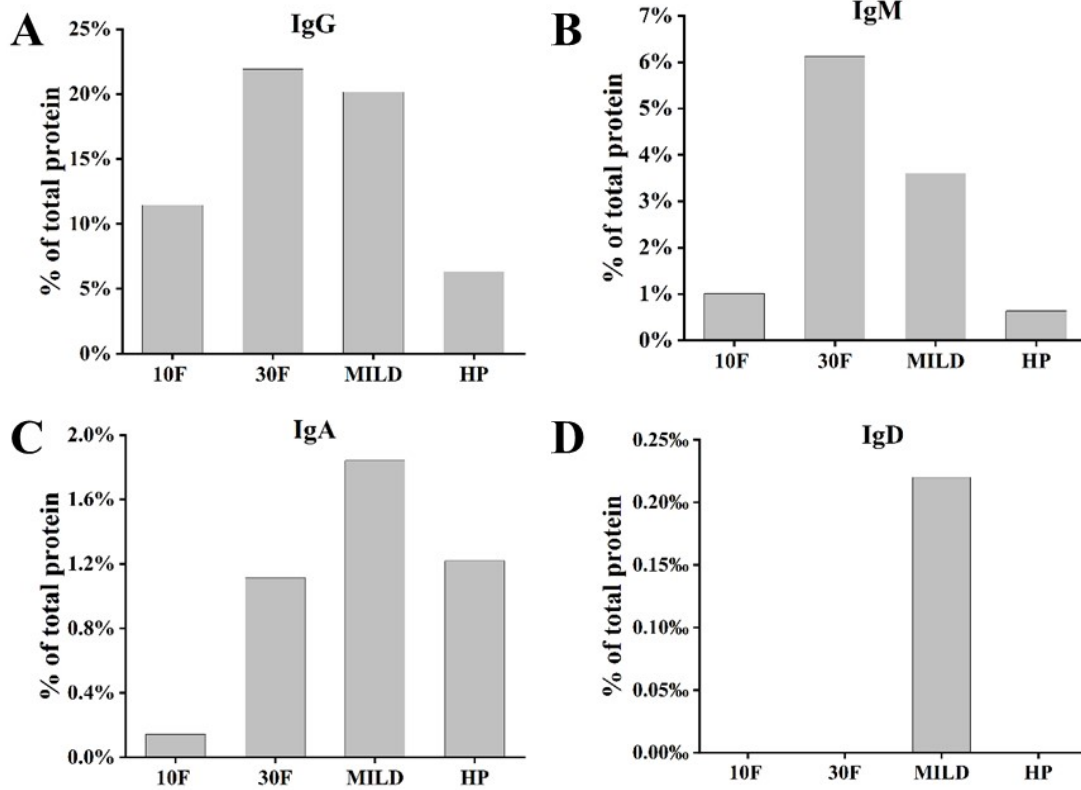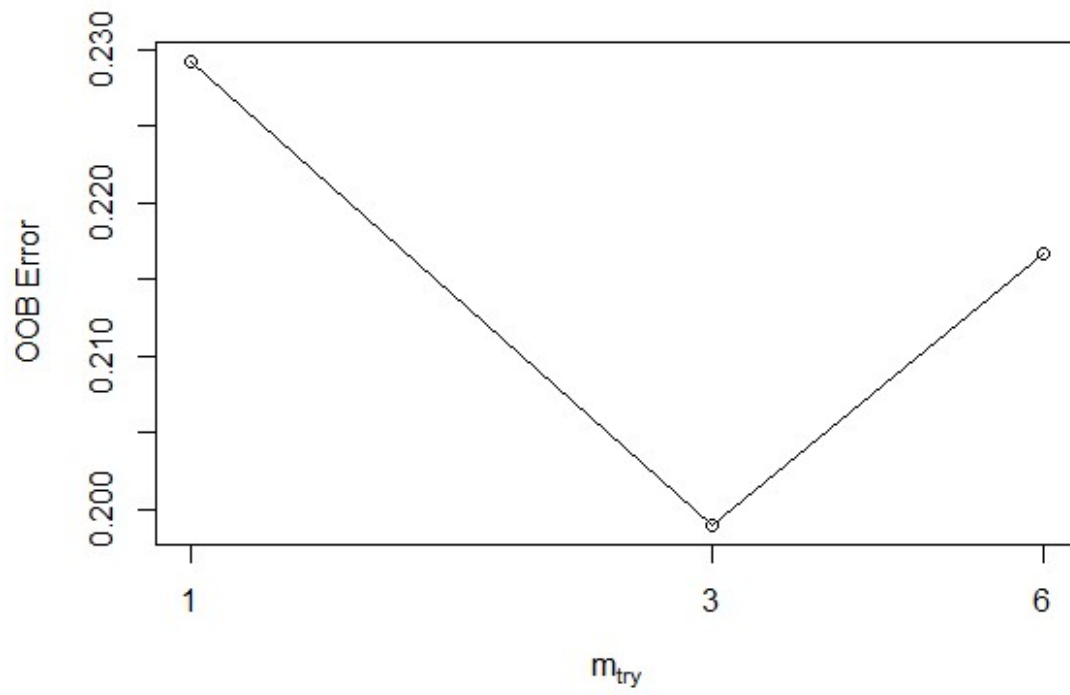
Supplemental Figure 4. Relative abundance of four immunoglobulins including IgG (A), IgM (B), IgA (C) and IgD (D) in the MXene-coronas.
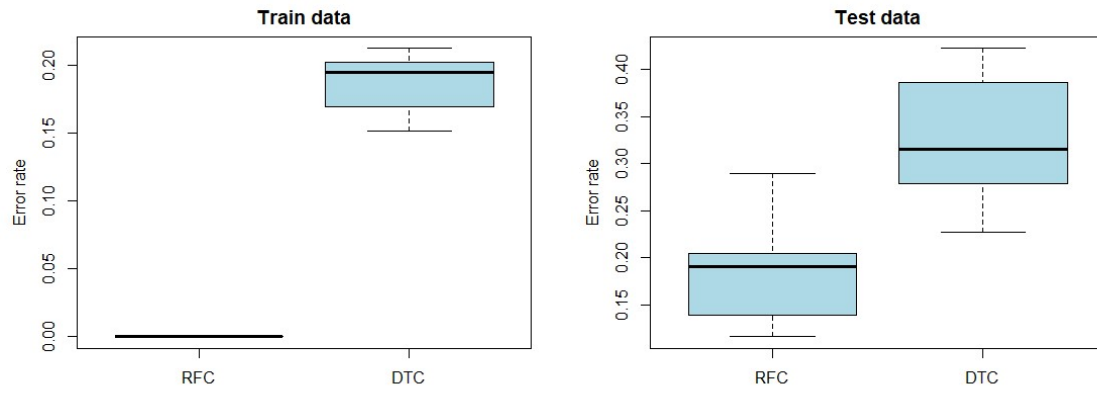
Supplemental Figure 5. Error rates of DTC and RFC models based on the train data (left)
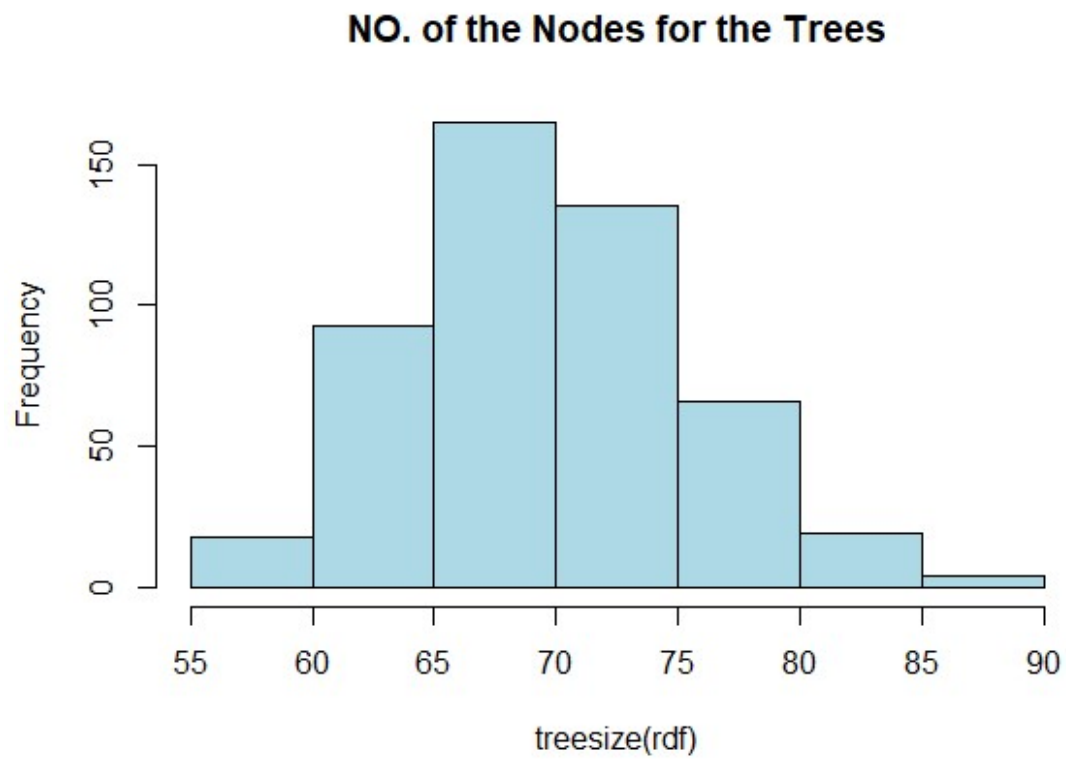
and the test data (right).
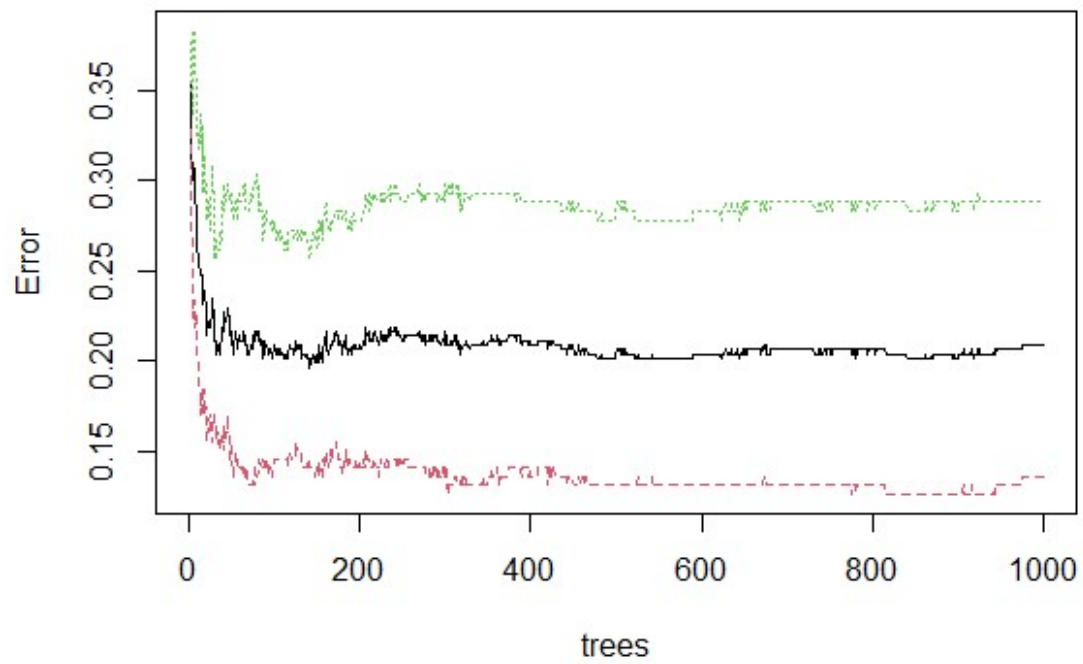
Supplemental Figure 6. Optimization of the parameter ntree. The ntree was selected to 500 in the finial model.

Supplemental Figure 7. Optimization of the parameter mtry. The mtry was selected to 3 in the finial model.

Supplemental Figure 8. The size distribution of decision trees in the trained RFC.
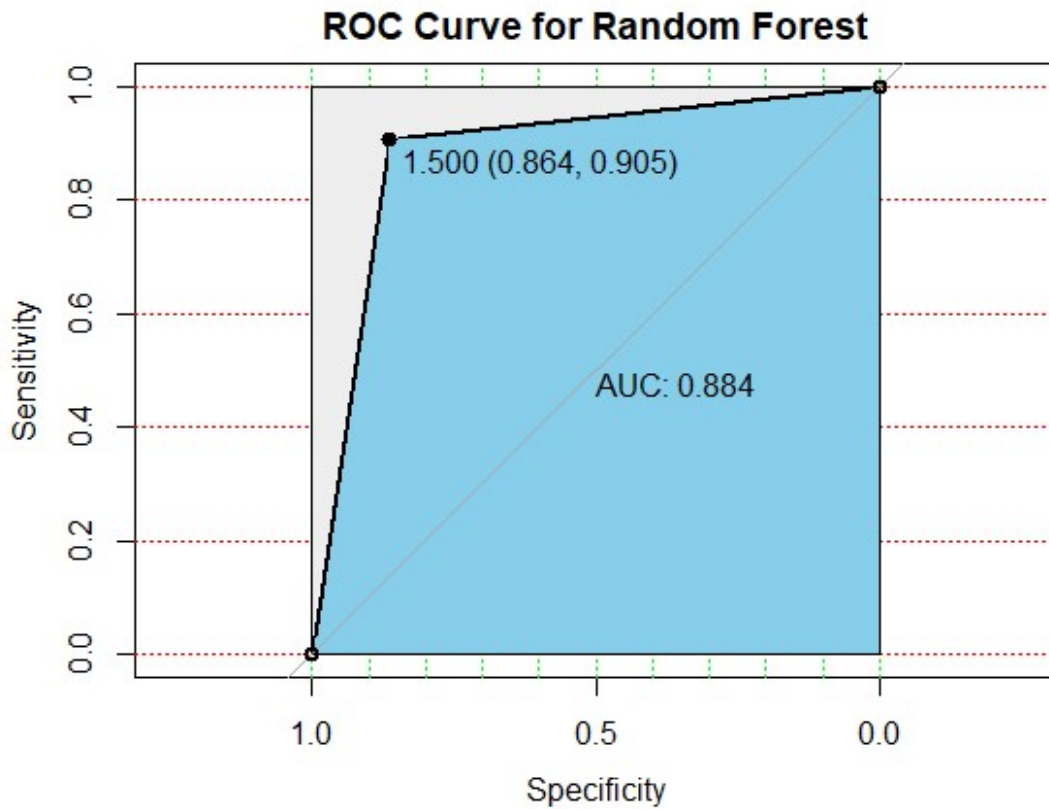
Supplemental Figure 9. ROC curve for random forest included in the final model. The area under the receiver operating curve (AUC) of the model is generally considered to be an indicator of the predictive power of model. With an AUC of 0.88, indicating the model performance is excellent.

Supplemental Table 1. Elemental composition on microparticles surface before and after immersion in HP by XPS.

Samples	Atomic (%)					
	Ti	C	Al	F	O	N
30F-Ti$_3$C$_2$T$_x$	27.52	32.43	0.93	14.63	24.50	--
MILD-Ti$_3$C$_2$T$_x$	21.87	32.38	2.26	14.46	29.03	--
30F-Ti$_3$C$_2$T$_x$@corona	5.31	59.46	0.43	4.02	19.14	11.64
MILD- Ti$_3$C$_2$T$_x$@ corona	6.70	50.75	0.57	6.59	22.07	13.33

Supplemental Table 2. Original data for the DLS characterization and zeta potential characterization corresponding to Table 1. Values are from six-nine independent experiments. Test in 0.02 M pH 7.4 PBS buffer at 25°C.

Samples	Size (nm)	Zeta potential
10F-Ti$_3$C$_2$T$_x$	438.8; 508.3; 452.8; 456.5	-22.3; -25.8; -24.0; -27.0
	420.3; 517.8; 435.4; 440.3; 467.4	-29.2; -32.5; -33.3; -32.5
30F-Ti$_3$C$_2$T$_x$	761.7; 823.8; 728.7; 912.3	-17.7; -18.6; -20.5; -22.1
	739.8; 834.1; 664.1; 860.6	-23.7; -23.0; -20.9; -22.4; -24.2
MILD-Ti$_3$C$_2$T$_x$	644.6; 740.6; 676.1	-25.3; -27.0; -29.9; -29.5
	725.1; 789.7; 759.4; 887.4	-31.1; -32.0; -30.7; -29.0
10F-Ti$_3$C$_2$T$_x$@corona	1766; 928.9; 1219	-7.3; -7.6; -8.8; -10.3
	894.8; 1059; 1325	-11.2; -11.2; -12.5; -13.8; -13.5
30F-Ti$_3$C$_2$T$_x$@corona	2272; 1209; 1419	-10.5; -10.7; -12.0; -12.5
	2062; 1610; 1526; 1320	-13.4; -14.0; -14.5; -15.0; -15.3
MILD-Ti$_3$C$_2$T$_x$@corona	2773; 2306; 2392; 2673	-9.1; -9.6; -11.4; -12.5
	2046; 2435; 2296; 1357; 2500	-14.1; -13.4; -15.0; -14.2; -15.8